JOURNAL OF SOLID STATE CHEMISTRY 38, 138–147 (1981)

Erratum

Volume **35,** No. 1 (1980), in the article, "Defect Structures in the Brannerite-Type Vanadates. I. Preparation and Study of $Mn_{1-x}\phi_xV_{2-2x}Mo_{2x}O_6$ ($0 \leq x \leq 0.45$)," Roman Kozłowski, Jacek Ziółkowski, Krzysztof Mocała, and Jerzy Haber, pp. 1–9: Pages 4 and 5 were transposed with pages 6 and 7. For the readers' convenience, the corrected article is reprinted beginning on the next page.

JOURNAL OF SOLID STATE CHEMISTRY 35, 1–9 (1980)

Defect Structures in the Brannerite-Type Vanadates. I. Preparation and Study of $Mn_{1-x}\phi_xV_{2-2x}Mo_{2x}O_6$ ($0 \leq x \leq 0.45$)

ROMAN KOZŁOWSKI, JACEK ZIÓŁKOWSKI,* KRZYSZTOF MOCAŁA, AND JERZY HABER

Institute of Catalysis and Surface Chemistry, Polish Academy of Sciences, ul. Niezapominajek, 30–239 Kraków, Poland

Received May 30, 1979

Phases of the formula $Mn_{1-x}\phi_xV_{2-2x}Mo_{2x}O_6$ with the brannerite-type (α) structure, where ϕ represents a vacancy at the Mn^{2+} site, have been sythesized and characterized by X-ray diffraction and DTA. The X-ray data are listed for MnV_2O_6 and solid solution with $x = 0.40$. They indicate the random distribution of V and Mo over the original V sites and the random distribution of Mn and vacancies over the original Mn sites. The monoclinic cell dilates with increasing x, primarily in the direction of the b-axis. The phase diagram of the pseudobinary MnV_2O_6–MoO_3 system has been determined. The extent of the stability region for the investigated brannerite solid solution has been established ($x_{max} = 0.45$ at 583°C). Other features determined in this system were: (a) little solubility of MoO_3 in the high-temperature (β) modification of MnV_2O_6, (b) a two-phase area of α- and β-type solid solution coexistence, (c) a eutectic point between α-type solid solution and MoO_3 at 583°C and 75 mole% of MoO_3 and (d) phase relationships at the liquidus.

Introduction

The recent research of Sleight, Aykan, and their co-workers (*1*, *2*) revealed that solid solution systems based on complex solvent oxide may exhibit high activity and selectivity in the partial oxidation of olefins. The work has involved the preparation of numerous scheelite-type phases of the formula $A_{1-x}\phi_xMO_4$, where ϕ represents a vacancy at cation site A, A = different univalent (Li, Na, Ag, Tl), divalent (Pb, Cd, Ca, Sr), and trivalent (Bi, Ce, La, Y) cations, and M is Mo^{6+}, W^{6+}, and/or V^{5+}.

The catalytic investigations showed that activity and selectivity in the reactions of propylene oxidation and ammoxidation increase rapidly with an increase in the defect concentration x. The best catalytic behavior was observed when cation site A was partially vacant and partially occupied by bismuth. The ESCA experiments revealed as well that the presence of vacancies brings about a considerably higher Bi concentration on the surface than in the bulk of the samples (*3*).

Similar concepts underlie the works with solid solutions based on perovskite systems initiated recently by Voorhoeve *et al.* (*4*, *5*).

In the present study we moved to a solid solution system based on the brannerite ($ThTi_2O_6$)-type structure (*6*) which is monoclinic with the space group $C2/m$. In this structure, which can be formulated as AB_2O_6, both cations A and B are octahedrally coordinated by six O atoms (see fig. 4 as well as the detailed description of the structure given later in this work). All A cations are in equivalent positions, as are the

* To whom correspondence should be addressed.

0022-4596/80/130001-09$02.00/0

B cations also. The structure is amenable to substitution of other cations if only the charge balance requirement is fulfilled. And thus, while brannerite itself contains tetravalent Th^{4+} and Ti^{4+} in *A* and *B* positions, respectively, a number of divalent metal vanadates of formula $M^{2+}V_2^{5+}O_6$ (where M = Mg, Co, Cd, Hg, Zn, Mn) adopt also brannerite or brannerite-related (Cu) structure (*7–11*).

A yet more complicated substitution scheme is to be found for $NaVMoO_6$ compound, where univalent Na^+ ions occupy the *A* positions whereas V^{5+} and Mo^{6+} are distributed at random over the *B* positions (*12*). Increasing the Mo^{6+}/V^{5+} ratio in this compound results in a deficiency of cations *A*. The phases may be described by the formula $Na_{1-x}\phi_xV_{1-x}Mo_{1+x}O_6$ with $0 \leq x \leq 0.30$ (*13*). In the same paper similar systems with Li ($0 \leq x \leq 0.16$), K ($0.18 \leq x \leq 0.24$), and Ag ($0 \leq x \leq 0.12$) have been described.

The reported data indicate that the brannerite structure is tolerant of cation vacancies in the *A* sites. By analogy it might be supposed that the similar *A*-cation-deficient phases are formed on substituting the Mo for V atoms in divalent metal brannerite vanadates.

Some preliminary syntheses performed in our laboratory revealed the extensive solid solubility of MoO_3 in MnV_2O_6 and CuV_2O_6, little solid solubility of MoO_3 in CoV_2O_6 and ZnV_2O_6, and no detectable solubility of MoO_3 in CdV_2O_6 and MgV_2O_6. The obtained solid solutions fit the general formula $Me^{2+}_{1-x}\phi_xV_{2-x}Mo_{2x}O_6$, where ϕ represents a vacancy at the Me^{2+} site.

Our primary focus has been on brannerite solid solutions based on MnV_2O_6 matrix. They contain a combination of Mo^{6+}, V^{5+}, and Mn^{2+} ions which are well-known components of selective oxidation catalysts, as well as vacancies. What is more, the solid solution principle enables one to investigate the effect of defect and solute ion concentrations, which can be systematically varied in the unchanged oxygen framework, on catalytic activity and selectivity. A program of catalytic research is at present underway and will be reported in detail in the future.

This paper presents the results of solid state investigations. A phase diagram of the pseudobinary MnV_2O_6–MoO_3 system was determined in order to establish the thermodynamic stability range of $Mn_{1-x}\phi_xV_{2-2x}Mo_{2x}O_6$ solutions. The synthesized samples of solid solutions were characterized by the X-ray method.

Solid solution samples will be labeled throughout this paper as *M*V followed by a numeral which specifies the mole percentage vanadium replaced by molybdenum in the MnV_2O_6 structure. This numeral is equal to $100x$. For example, *M*V-20 corresponds to the chemical formula $Mn_{0.80}\phi_{0.20}V_{1.60}Mo_{0.40}O_6$.

Experimental

The solid solutions under study were prepared by solid state reactions between Mn_2O_3, V_2O_5, and MoO_3. V_2O_5 and MoO_3 were p.a.-grade commercial oxides. Mn_2O_3 was obtained by pyrolysis of $MnCO_3$ at 700°C. The reaction mixtures were prepared by weighing out the oxides in the appropriate molar ratios followed by thorough grinding in a mortar. The mixtures were air heated using alumina crucibles. During heating samples were periodically removed, cooled, and ground to ensure complete reaction. An elemental analysis of two solid solution samples (*M*V-0 and *M*V-40) was carried out after final calcination, using atomic absorption spectroscopy. They were found to have the assumed stoichiometry within the error of analytical method (±1% in the absolute weight of the metals), which indicates that there is no loss of components in the course of heating.

A summary of the preparation parameters is given in Table I. Compositions of solid solutions obtained were determined from the

TABLE I

EXPERIMENTAL CONDITIONS FOR PREPARATION OF $Mn_{1-x}\phi_xV_{2-2x}Mo_{2x}O_6$ COMPOUNDS

Stiochiometry of the initial oxide mixtures expressed by x-parameters	Calcination condition[a]	Phase composition of products	Position of (020) X-ray line (Å)
0.00	H	*M*V-0	1.7658
0.02	S_1	*M*V-2 + (V_2O_5 + Mn_2O_3) as minor constituents	1.7684
0.05	S_1	*M*V-5 + (V_2O_5 + Mn_2O_3) as minor constituents	1.7722
0.10	S_2	*M*V-10	1.7787
0.15	S_3	*M*V-15	1.7834
0.18	H	*M*V-18	1.7858
0.20	H	*M*V-20	1.7874
0.25	H	*M*V-25	1.7925
0.27	H	*M*V-27	1.7939
0.30	H	*M*V-30	1.7959
0.34	H	*M*V-34	1.8003
0.36	H	*M*V-36	1.8023
0.38	H	*M*V-38	1.8049
0.40	H	*M*V-40	1.8065
0.42	H	*M*V-42 + traces of MoO_3	1.8091
0.44	H	*M*V-42 + MoO_3	1.8091

[a] S_1, S_2, and S_3 indicate stepwise calcination for 20 hr consecutively at 2 × 520, 540, 560, and 580°C (S_1), 2 × 520, 540, 560, 580, and 3 × 600°C (S_2), and 2 × 520, 540, 560, 580, and 600°C (S_3). H indicates calcination at 600°C for 40 hr.

shifts of the "brannerite" (020) line on X-ray diagrams (see respective passage under Results). The selection of the appropriate preparation variables has been done on the basis of a detailed study of the solid solution formation mechanism. The results of this study are reported elsewhere (*14*).

Our attempts to prepare the single-phase samples with $x < 0.10$ remained unsuccessful, as the applied temperatures of final calcination, which could not surpass the upper limit of the brannerite phase stability field (see the phase diagram), proved to be insufficiently high to ensure complete reaction of the oxide mixtures. We decided therefore, to include in the studied series two preparations from the low-MoO_3 region which contained small amounts of unchanged V_2O_5 and Mn_2O_3.

Pure MnV_2O_6 was also prepared by the "wet" method. It consisted of precipitation of hydrated precursor from water solutions of equimolar mixtures of manganese nitrate and ammonium metavanadate followed by filtration, washing out with water, drying at 120°C, and annealing at 500°C for 5 hr.

DTA curves were recorded with a Setaram M-5 microanalyzer in a stream of purified air, at a heating rate of 10 and 1.5°C/min. The preparations studied were found to creep after melting over the surface of the Pt crucible and to corrode the very fine thermocouple wires of the sample holder. As a result it was decided to build a special sample holder in which thermocouples were protected in the manner shown in Fig. 1. Samples of 140 mg were placed in Pt crucibles. Al_2O_3 preheated at 1500°C for 24 hr and Brazilian quartz (transition temperature 573°C) were used as references. On constructing the phase diagram the onset temperatures or peak temperatures were taken to determine

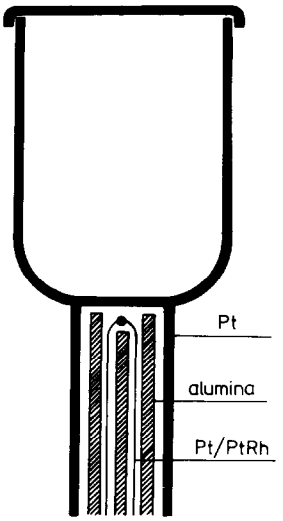

FIG. 1. DTA crucible–thermocouple contact.

the solidus and liquidus lines, respectively, the accuracy being ±2°C.

The X-ray diffraction patterns were obtained with a DRON-2 X-ray diffractometer with Cu$K\alpha$ radiation and an internal standard of Al ($a = 4.0494$ Å at 25°C). The phase identification was based upon the published patterns of Mn_2O_3, V_2O_5, MoO_3, $MnMoO_4$, and $Mn_2V_2O_7$ (*15*). Cell dimensions were refined by the least-squares method. X-Ray intensity data were collected for pure MnV_2O_6 and *M*V-40. We have found our samples to be very sensitive to preferred orientation which brings about a strong increase in the intensity of ($h0l$) reflections and a decrease in the intensity of reflections with $k \neq 0$ as compared to the calculated intensities. This indicates easy cleavage planes parallel to the *b*-axis. A special sample preparation technique was applied to avoid preferred orientation. It included passing the ground powder through 400-mesh screen placed over a flat quartz sample holder covered with paraffin oil. The grains fall down and adhere to the plate, producing an entirely unoriented sample layer. The plate was sufficiently large to intercept all X rays over the entire θ range. The X-ray pattern was scanned in the range of 2θ from 13.5 to 70° at 0.5°/min and peak surface areas were measured with a planimeter.

Results and Discussion

Phase Diagram

A series of the investigated solid solutions may be represented formally as $Mn_{1-x}V_{2-2x}Mo_{2x}O_6 = (1-x)MnV_2O_6 + (2x)MoO_3$. From this it can be seen that the solid solution extends along the MnV_2O_6–MoO_3 line which constitutes a pseudobinary section of the ternary system MnO–V_2O_5–MoO_3. The phase diagram of the MnV_2O_6–MoO_3 system was thus constructed in order to evaluate the maximum value of x for a single-phase brannerite and to determine the field of thermodynamic stability of solid solution.

The materials used for these studies were:

1°, the samples listed in Table I in the $0 \leq x \leq 0.42$ range;

2°, mixtures of *M*V-42 and MoO_3 in the $x > 0.44$ part of the system.

The phase diagram was determined with DTA, visual observations, and X-ray investigations carried out in a high-temperature camera or after quenching the samples in air to room temperature. It is shown in fig. 2. Features marked on the diagram by solid lines can be regarded as well established (±2°C) and those by broken lines as tentative.

The end member compound MnV_2O_6 is known to undergo a phase transformation at about 550°C (*16*). In this study the transition temperature was found to be 540°C. The low-temperature polymorph of brannerite structure type is referred to as α-form and the other, stable above 540°C, is referred to as β-form. The phase transformation is reversible. β-MnV_2O_6 gives a characteristic X-ray pattern with $d = 4.76$, 4.37, 3.54, 3.37, 3.10, 2.918, 2.380, 2.245, 1.940, 1.877, 1.850, 1.807, 1.497, 1.475, and

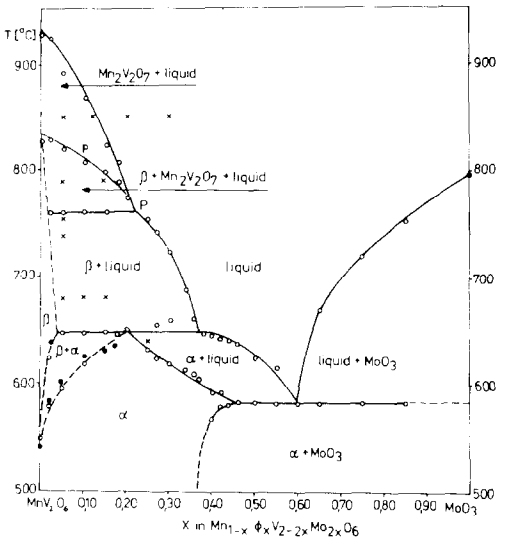

FIG. 2. The system MnV_2O_6–MoO_3. ○, DTA; ●, X-ray high-temperature camera observations; x, phase identification after air quenching.

1.461 Å, as registered at 600°C. β-MnV_2O_6 melts incongruently at 825°C, decomposing to $Mn_2V_2O_7$ and liquid. On further heating the liquidus line is crossed over at 935°C.

The outstanding feature of the diagram is the very large region of α-form solid solution which extends to about 62 mole% of MoO_3 ($x = 0.45$) at 583°C. The extent of solid solubility of MoO_3 in β-MnV_2O_6 is very small and does not exceed 8 mole% ($x = 0.04$). There is a temperature dependence for the maximum Mo concentration tolerated in the α- and the β-form, respectively. α and β solid solutions coexist in the temperature range 540–650°C in the MoO_3-poor ($x < 0.20$) portion of the system. The diagram includes one eutectic between α-*M*V-45 and MoO_3 at 583°C and 75 mole% of MoO_3 ($x = 0.60$).

α-*M*V-20, which reveals the highest thermal stability among α-type solid solutions, melts incongruently at 650°C, decomposing to almost nondefect β-MnV_2O_6 (exactly to β-*M*V-4) and liquid containing about 54 mole% MoO_3 ($x = 0.37$). Above this temperature a melt and a slightly defect β-phase coexist up to the temperature of 760°C. At higher temperatures β-phase decomposes partly, and above the p-line completely, to MnV_2O_7 and liquid, the p-line being the projection of the peritectic line joining in the space of the ternary MnO–V_2O_5–MoO_3 diagram two peritectic points: one, representing the composition of a liquid remaining in equilibrium with MnV_2O_6 and $Mn_2V_2O_7$ in the MnO–V_2O_5 system, and the other, P in the MnV_2O_6–MoO_3 system. It should be recalled at this point that as the investigated system is merely a pseudobinary section of the ternary MnO–V_2O_5–MoO_3 system, the appearance of $Mn_2V_2O_7$, whose composition does not fall on the MnV_2O_6–MoO_3 axis, is fully justifiable.

X-Ray Measurements

Gondrand *et al.* have reported that MnV_2O_6 belongs to the brannerite structure type (*10*). However, no X-ray data were given.

In the present study pure MnV_2O_6 was obtained either by annealing of an oxide mixture of composition $Mn_2O_3 + 2V_2O_5$ or by precipitation. In both cases a pure product free from residual oxides or other vanadates was obtained. It gave an X-ray pattern similar to those reported for β-CdV_2O_6 (*8*) and ZnV_2O_6 (*9*), and to that of MgV_2O_6 calculated from published single-crystal data (*7*). MnV_2O_6 was therefore taken to belong to the class of compounds with brannerite-type structure and the powder pattern was indexed accordingly (Table II). The calculated cell parameters are:

$$a = 9.315(3)\ \text{Å}, \quad b = 3.536(1)\ \text{Å},$$
$$c = 6.754(2)\ \text{Å}, \quad \beta = 112.66(2)°.$$

The intensities of diffraction maxima were calculated with the use of atomic positional parameters identical to those of MgV_2O_6 and with the use of atomic scattering factors for Mn^{2+}, V^{5+}, and O^- (*17*). Of the 40 possible peaks, which could have been observed, 31

TABLE II

X-RAY POWDER DIFFRACTION DATA FOR MnV_2O_6[a] (*MV*-0) AND $Mn_{0.6}V_{1.2}Mo_{0.8}O_6$[b] (*MV*-40)

MV-0					*MV*-40				
hkl (1)	d_{obs} (Å) (2)	d_{calc} (Å) (3)	I_{obs} (4)	I_{calc} (5)	d_{obs} (Å) (6)	d_{calc} (Å) (7)	I_{obs} (8)	I_{calc} (9)	*hkl* (10)
001	6.25	6.23	57	7	6.27	6.26	606	380	001
$20\bar{1}$	4.43	4.42	143	223	—	4.44	—	58	$20\bar{1}$
200	4.31	4.30	58	30	4.35	4.34	379	367	200
110	3.28	3.27	607	560	3.24	3.34	488	466	110
$20\bar{2}$	3.16	3.17	678	654	3.17	3.17	775	759	$20\bar{2}$
$11\bar{1}$	3.09	3.09		196	3.14	3.14		848	$11\bar{1}$
002		3.09		6		3.13		11	002
			215	202			817	859	
201	3.04	3.03	678	739	3.08	3.07	842	881	201
111	2.737	2.736	485	585	2.782	2.781	463	609	111
$11\bar{2}$	2.442	2.442	71	38	2.468	2.468	118	55	$11\bar{2}$
$31\bar{1}$	2.329	2.329		271	2.357	2.359	328	356	$31\bar{1}$
$40\bar{1}$		2.326		126	2.344	2.344	67	74	$40\bar{1}$
			357	397					
$20\bar{3}$	—	2.239	—	5	—	2.240	—	15	$20\bar{3}$
310	2.227	2.226	64	87	—	2.259	—	0	310
$40\bar{2}$	2.213	2.212	100	87	2.220	2.220	261	269	$40\bar{2}$
202	2.161	2.158	86	48	2.178	2.178		114	202
400	2.152	2.149	79	58		2.171		35	400
							210	149	
$31\bar{2}$	2.140	2.140	78	62	—	2.159	—	14	$31\bar{2}$
112	—	2.107	—	20	2.133	2.133	160	186	112
003	2.079	2.078	214	176	2.086	2.086	236	225	003
311	1.919	1.922	121	112	1.949	1.949	76	71	311
$40\bar{3}$	1.901	1.905	143	154	1.907	1.907	109	140	$40\bar{3}$
$11\bar{3}$	1.883	1.883	157	160	1.897	1.897	93	123	$11\bar{3}$
401	—	1.826	—	5	1.847	1.847	42	53	401
$31\bar{3}$	—	1.814	—	11	1.824	1.824	93	87	$31\bar{3}$
020	1.768	1.768	286	324	1.806	1.807	354	399	020
021	—	1.701	—	0	1.736	1.736	51	28	021
$20\bar{4}$	1.688	1.688	57	61	1.690	1.690	76	45	$20\bar{4}$
					—	1.673	—	6	$22\bar{1}$
					1.664	1.668		55	220
113	1.649	1.648	164	125		1.664		127	113
							236	182	
$22\bar{1}$		1.642		24	—	1.653	—	9	203
203	1.640	1.639		0	—	1.657	—	1	$51\bar{1}$
$51\bar{1}$		1.639		7	—	1.642	—	6	$51\bar{2}$
			57	31	1.619	1.619	109	152	312
						1.585	—	38	$40\bar{4}$

TABLE II—*Continued*

MV-0					*MV*-40				
hkl (1)	d_{obs} (Å) (2)	d_{calc} (Å) (3)	I_{obs} (4)	I_{calc} (5)	d_{obs} (Å) (6)	d_{calc} (Å) (7)	I_{obs} (8)	I_{calc} (9)	*hkl* (10)
220	—	1.635	—	5					
312	1.599	1.599	86	123	1.565	1.569		185	$22\bar{2}$
$40\bar{4}$	1.583	1.584	36	33		1.566		164	510
						1.565		3	022
								18	004
						1.565	303	371	
004	—	1.558	—	1	1.556	1.557		73	$60\bar{2}$
						1.556		224	221
$60\bar{2}$	1.547	1.547		67			286	297	
510		1.546		119					
$22\bar{2}$		1.544		145					
			357	331					
022	1.538	1.538	—	2					
$60\bar{1}$	1.530	1.531		21	1.544	1.543	76	74	$60\bar{1}$
221		1.528		164					
			178	185					
					1.534	1.533	93	90	402
$51\bar{3}$	1.517	1.518		272	1.527	1.526	354	336	$51\bar{3}$
402		1.517		72					
			400	344					
$31\bar{4}$	1.506	1.506	121	119	1.512	1.512	135	157	$31\bar{4}$
$11\bar{4}$	—	1.494	—	6	1.503	1.503	42	52	$11\bar{4}$
$60\bar{3}$	—	1.474	—	10	—	1.480	—	7	$60\bar{3}$
600	1.433	1.433	136	52	1.448	1.448	50	54	600

[a] Cell parameters: $a = 9.315(3)$ Å, $b = 3.536(1)$ Å, $c = 6.754(2)$ Å, $\beta = 112.66(2)°$.
[b] Cell parameters: $a = 9.378(3)$ Å, $b = 3.613(1)$ Å, $c = 6.751(2)$ Å, $\beta = 112.18(2)°$.

were judged to be observed. R of 0.15 was obtained from these 31 observations, R being defined as $\sum|I_o - I_c|/\sum I_o$. The intensities of the unobserved reflection were calculated and are given in Table II.

The brannerite phases in the Mn–V–Mo–O system can be represented by the general formula $Mn_{1-x}\phi_x V_{2-2x}Mo_{2x}O_6$. The proposed formulation implies the substitution of Mo^{6+} ions for V^{5+} ions in the brannerite structure with the removal of an equivalent number of Mn^{2+} ions and the generation of the same number of vacancies at Mn^{2+} lattice sites.

In order to confirm the postulated substitution mechanism one sample of composition $Mn_{0.60}Mo_{0.80}V_{1.60}O_6$ (*M*V-40), i.e., exhibiting the greatest practically attainable departure from the initial MnV_2O_6 stoichiometry, was chosen for structure analysis using X-ray diffraction data.

The intensities of diffraction maxima were calculated as described above assuming the random distribution of Mo atoms, over the

lattice positions of V^{5+}, and of vacancies, over the lattice positions of divalent metal atoms, in a structure of brannerite type. The observed and calculated intensities are compared in Table II; the R value is 0.13 for 32 independent observations of 42 possible peaks. No attempts to refine the positional parameters of atoms in the analyzed structures were undertaken in view of the small number of symmetry-independent reflections which could be observed from the powder. This is reflected in rather large R values for both pure and highly substituted MnV_2O_6 (for well-established structures R generally does not exceed 0.05). The detailed structure analysis based on single-crystal data would be highly desirable. However, if we compare the *observed* intensities of MnV_2O_6 and MV-40 we find that the substitution affects to a great extent the intensities of diffraction maxima, this being especially evident for planes (001), (201), (200), (111), and (002). The intensities calculated on the basis of assumed solid solution structure, though with the use of unrefined, approximate coordinates of atomic positions, reflect reasonably well these changes, supporting the suggested substitution scheme.

Figure 3 shows variation in cell parameters a, b, c, β, and $c \sin \beta$ with the parameter x,

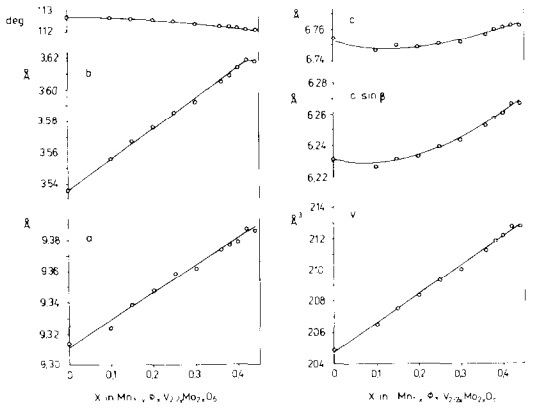

FIG. 3. Cell parameters and cell volume vs x in the $Mn_{1-x}\phi_x V_{2-2x}Mo_{2x}O_6$.

i.e., with Mo^{6+} content and vacancy concentration. It can be seen that the cell parameters a and b increase linearly whereas $c \sin \beta$ increases nonlinearly with increasing x. This is to be expected since Mo^{6+} (r = 0.60 Å) is significantly larger than V^{5+} (r = 0.54 Å) (*18*), and also, since vacancies cause an outward displacement of the neighboring oxygen ions behaving thus like an ion of larger size, leading to an increase in the lattice parameters.

The dilations of the parameters of R-40 with respect to pure MnV_2O_6 phase amount to: $\Delta a = 0.68\%$, $\Delta b = 2.16\%$, $\Delta c \sin \beta = 0.46\%$.

The highest dilatation of the lattice occurs in the direction of the b-axis. Again, this might be considered the expected trend taking into account the crystal structure of the brannerite type. It can be described as composed of BO_6 octahedra which share opposite corners forming chains running parallel to the b-axis (Fig. 4). Octahedra in adjacent chains share edges forming anionic sheets parallel to the (001) plane. A ions are situated between anionic sheets so that each A ion is coordinated by six O atoms arranged in a distorted octahedron. AO_6 share edges forming chains paralleling the b-axis. These chains are not linked to one another; they provide a rather open structure between the BO_6 sheets. The substitution of Mo^{6+} for V^{5+} and the generation of cationic vacancies at

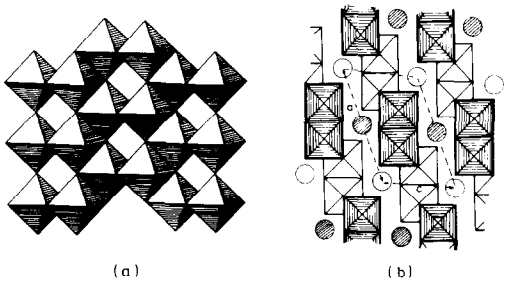

FIG. 4. The brannerite-type structure (after (*6*)). (a) A sheet of BO_6 octahedra; (b) idealized projection of the structure on the ac-plane.

Mn^{2+} sites in the MnV_2O_6 network should contribute primarily to an elongation of VO_6, MnO_6 chains parallel to the *b*-axis with slight overall dilatation of the lattice in the *ac*-plane.

As can be calculated from Table II the (020) reflection shows the greatest shift in 2θ value with the substitution degree *x*. The position of this reflection can be, thus, used to determine *x* in a solid solution of unknown composition, the accuracy of the determination being ± 0.01.

Conclusions

The brannerite structure is particularly tolerant of cation vacancies in the *A* sites. In the $A_{1-x}\phi_x V_{1-x}Mo_{1+x}O_6$ compounds, where *A* = Li, Na, K, Ag, 12% (Li) to 30% (Na) of these sites can be vacant (*13*). In this work we find that the limit for $Mn_{1-x}\phi_x V_{2-2x}Mo_{2x}O_6$ system is as high as 45%. Further solid state research is being carried out on analogous phases with divalent cations other than Mn^{2+}.

Acknowledgment

The authors wish to express their gratitude to Dr. T. Machej for constructing the DTA sample holder and for his helpful assistance in some experiments.

References

1. K. AYKAN, D. HALVORSON, A. W. SLEIGHT, AND D. B. ROGERS, *J. Catal.* **35**, 401 (1974).
2. A. W. SLEIGHT, K. AYKAN, AND D. B. ROGERS, *J. Solid State Chem.* **13**, 231 (1975).
3. A. W. SLEIGHT AND W. J. LINN, *Ann. N.Y. Acad. Sci.* **272**, 22 (1976).
4. R. J. H. VOORHOEVE, J. P. REMEIKA, L. E. TRIMBLE, A. S. COOPER, F. J. DISALVO, AND P. K. GALLAGHER, *J. Solid State Chem.* **14**, 395 (1975)
5. R. J. H. VOORHOEVE, J. P. REMEIKA, AND L. E. TRIMBLE, *Ann. N.Y. Acad. Sci.* **272**, 3 (1976).
6. R. RUH AND A. D. WADSLEY, *Acta Crystallogr.* **21**, 974 (1966).
7. H. N. NG AND C. CALVO, *Canad. J. Chem.* **50**, 3619 (1972).
8. J. C. BOULOUX AND J. GALY, *Bull. Soc. Chim. Fr.*, 736 (1969).
9. J. ANGENAULT, *Rev. Chim. Miner.* **7**, 651 (1970).
10. M. GONDRAND, A. COLLOMB, J. C. JOUBERT, AND R. D. SHANNON, *J. Solid State Chem.* **11**, 1 (1974).
11. C. CALVO AND D. MANOLESCU, *Acta Crystallogr. Sect. B* **29**, 1743 (1973).
12. B. DARRIET AND J. GALY, *Bull. Soc. Fr. Mineral. Cristallogr.* **91**, 325 (1968).
13. J. GALY, J. DARRIET, AND B. DARRIET, *C. R. Acad. Sci. Paris Ser. C* **264**, 1477 (1967).
14. J. ZIÓŁKOWSKI, R. KOZŁOWSIKI, K. MOCAŁA, AND J. HABER, *J. Solid State Chem.*, in press.
15. ASTM POWDER DIFFRACTION FILE, 10–69, 9–387, 5–508, 18–783, 22–436 (1972).
16. G. M. CLARK AND A. N. PICK, *J. Thermal Anal.* **7**, 290 (1975).
17. "INTERNATIONAL TABLES FOR X-RAY CRYSTALLOGRAPHY," Vol. IV, pp. 72–97, Kynoch Press, Birmingham (1974).
18. R. D. SHANNON AND C. T. PREWITT, *Acta Crystallogr. Sect. B* **25**, 925 (1969).